Wagener, T., Goda, K., Erdik, M., Daniell, J., & Wenzel, F. (2016). A spatial correlation model of peak ground acceleration and response spectra based on data of the Istanbul Earthquake Rapid Response and Early Warning System. Soil Dynamics and Earthquake Engineering, 85, 166-178. DOI: 10.1016/j.soildyn.2016.03.016

A Spatial Correlation Model of Peak Ground Acceleration and Response Spectra Based on Data of the Istanbul Earthquake Rapid Response and Early Warning System

Thomas Wagener[a], Katsuichiro Goda[b], Mustafa Erdik[c], James Daniell[d] and Friedemann Wenzel[e]

[a] Karlsruhe Institute of Technology, (KIT), Hertzstr. 16, Karlsruhe 76187, Germany
E-mail address: th.j.wagener@gmail.com

[b]University of Bristol, Queen's Building, University Walk, Bristol, BS8 1TR, United Kingdom
Tel: 44+1173315516
E-mail address: katsu.goda@bristol.ac.uk

[c]Earthquake Engineering Bogazici Univ., Kandilli Observatory and Earthquake Research Institute, Department of Earthquake Engineering, 81220,
Cengelkoy, Istanbul, Turkey, E-mail address: erdik@boun.edu.tr

[d] Karlsruhe Institute of Technology, (KIT), Hertzstr. 16, Karlsruhe 76187, Germany
E-mail address: james.daniell@kit.edu

[e] Karlsruhe Institute of Technology, (KIT), Hertzstr. 16, Karlsruhe 76187, Germany
Te: +49-721-608-44431.
E-mail address: friedemann.wenzel@kit.edu

Corresponding author: Friedemann Wenzel

Keywords: Ground Motion, Spatial Correlation, Istanbul Rapid Response and Early Warning System, Earthquake Loss

Abstract

Ground motion intensity measures such as the peak ground acceleration (PGA) and the pseudo spectral acceleration (PSA) at two sites due to the same seismic event are correlated. The spatial

correlation needs to be considered when modeling ground-motion fields for seismic loss assessments, since it can have a significant influence on the statistical moments and probability distribution of aggregated seismic loss of a building portfolio.

Empirical models of spatial correlation of ground motion intensity measures exist only for a few seismic regions in the world such as Japan, Taiwan and California, since for this purpose a dense observation network of earthquake ground motion is required. The Istanbul Earthquake Rapid Response and Early Warning System (IERREWS) provides one such dense array with station spacing of typically 2 km in the urban area of Istanbul. Based on the records of eight small to moderate (M_w3.5 – M_w5.1) events, which occurred since 2003 in the Marmara region, we establish a model of intra-event spatial correlation for PGA and PSA up to the natural period of 1.0 s.

The results indicate that the correlation coefficients of PGA and short-period PSA decay rapidly with increasing interstation distance, resulting in correlation lengths of approximately 3-4 km, while correlation lengths at longer natural periods (above 0.5 s) exceed 6 km. Finally, we implement the correlation model in a Monte Carlo simulation to evaluate economic loss in Istanbul's district Zeytinburnu due to a M_w7.2 scenario earthquake.

1. Introduction

In probabilistic and deterministic earthquake loss assessments, prediction of ground motion intensities is critically important [1]. For a given earthquake scenario, intensity distributions can be modeled by Ground Motion Prediction Equations (GMPE) in the form of ground motion parameters such as the peak ground acceleration (PGA), the peak ground velocity (PGV) and the pseudo-spectral acceleration (PSA). The uncertainty in these predictions is often represented by the between-earthquake (inter-event) variability and the within-earthquake (intra-event) variability [2]. The latter indicates that the extent of ground shaking at different sites shows individual scattering around the event median. When comparing recorded earthquake motion with a prediction model, it is observed that the intra-event residuals are spatially correlated and that the correlation decreases with increasing separation distance between two sites. In the past, this issue has been empirically investigated by using strong motion records from Japan, California, Taiwan and Italy [2-6]. It has been reported that intra-event correlation results in greater variability in the estimates of aggregate earthquake loss due to a single earthquake scenario [1]. Other studies have shown that intra-event spatial correlation can have a significant influence on the probability distribution of aggregate seismic losses [7] and specifically that rare losses are underestimated when spatial correlation is ignored [8].

Istanbul is a mega-city which is exposed to high seismic hazard, located close to the Marmara Fault, a part of the North Anatolian Fault, where a large earthquake of $M_w \geq 7$ occurring in the next 30 years is expected with a probability of more than 40% [9]. Particularly after the 1999 Izmit and Düzce Earthquakes, major efforts have been made by scientists and engineers to assess the earthquake hazard and vulnerability in Istanbul. A dense array of more than 100 strong motion recorders, making up the Istanbul Rapid Response and Early Warning System (IERREWS) has been installed in the urban area for rapid response and early warning purposes.

This dense array with an average station-spacing of 2-3 km provides a suitable basis to develop a regional spatial correlation model, which is currently lacking. Since 2003, eight small-to-moderate events (M_w3.5 - M_w5.1) with epicenters in the Marmara region have been recorded by stations of the IERREWS. Based on those records, we develop an intra-event spatial correlation model of PGA and PSA up to the natural period of 1.0 s for the urban area of Istanbul. To analyze the impact of the proposed correlation model on seismic risk assessments, we then implement this model in a Monte Carlo simulation to estimate seismic loss in Istanbul's district Zeytinburnu due to a scenario event occurring south of Istanbul in the Marmara Sea.

This work is structured as follows: First, we briefly summarize how spatial variability of ground motion parameters is characterized and how a spatial correlation model can be established by using recorded ground motion data. Subsequently, we present the IERREWS and the ground motion data which we use to establish the correlation model for the Istanbul area. A summary of the ground-motion data processing is given. The PGA and PSA from the processed acceleration time-histories are then used to evaluate the intra-event spatial correlation based on the ground motion model by Akkar and Bommer [10]. Finally, we implement the correlation model in a Monte Carlo simulation to estimate economic loss in Istanbul's district Zeytinburnu due to a M_w7.2 scenario earthquake.

2. Spatial Variability and Correlation of Ground Motion Parameters

GMPEs relate the logarithm of a ground motion parameter, such as PGA and PSA, at a site to the earthquake magnitude *M*, the distance *R* between earthquake source and site, other source properties and site effects (often modeled by the average shear-wave velocity in the upper 30 m below the surface V_{S30}):

$$ln\,(GMP) = f\,(M, R, source, site) + \eta + \varepsilon \qquad (1)$$

where GMP is the ground motion parameter whose median is predicted by the function *f*. The uncertainty in the prediction is modeled by the inter-event variability η and the intra-event

variability ε, which are assumed to be independent and normally distributed with zero mean and standard deviations σ_η and σ_ε, respectively.

The inter-event component indicates that the radiated energy released during the rupture process can vary even for the same modeled source parameters, resulting in systematically higher or lower intensities across all sites. The intra-event component represents the individual scattering at different sites due to different propagation paths and local site conditions, which remains after removing the inter-event residual. The total residual ε_T at a specific site is the sum of inter-event and intra-event residuals:

$$\varepsilon_T = \varepsilon + \eta \qquad (2)$$

with the total standard deviation:

$$\sigma_T = \sqrt{\sigma_\eta^2 + \sigma_\varepsilon^2} \qquad (3)$$

Since the inter-event residual η is constant for a single event, an inter-event correlation coefficient ρ_η can be defined as the ratio between inter-event variability and total variability [11]:

$$\rho_\eta = \frac{\sigma_\eta^2}{\sigma_\eta^2 + \sigma_\varepsilon^2} \qquad (4)$$

The similarity of ground motions at close sites due to their proximity can be described by a distance-dependent intra-event correlation coefficient $\rho_\varepsilon(\Delta)$. At zero separation distance, the site-to-site correlation must equal 1 while with increasing separation distance, it is expected to decay from 1. The intra-event spatial correlation can be empirically investigated for a specific region if a dense observation of earthquake ground motion is available. The total correlation coefficient is then [11]:

$$\rho_T(\Delta) = \rho_\eta + \frac{\sigma_\eta^2}{\sigma_\eta^2 + \sigma_\varepsilon^2}\rho_\varepsilon(\Delta) \qquad (5)$$

Intra-event correlations of ground motion parameters are available for specific seismic regions such as Japan [3, 5, 12], Taiwan [3, 11], California [4] and Europe [6,28].

3. Analysis procedure to evaluate intra-event correlation

To estimate the spatial correlation structure of a ground motion parameter in a specific area, the correlation of intra-event residuals, derived from earthquake recordings in the area, can be investigated. The following procedure can be adopted [13]:

1. Calculate the intra-event residuals ε for a given event using a suitable GMPE.

2. Construct pairs of intra-event residuals (ε_i, ε_j) and calculating their differences

$$\varepsilon_d = \varepsilon_i - \varepsilon_j \quad (6)$$

3. Assess the sample semivariogram:

$$\hat{\gamma}(\Delta) = \frac{1}{2}\sigma_d^2(\Delta) \quad (7)$$

where $\sigma_d^2(\Delta)$ is the variance of $\varepsilon_d(\Delta)$ that falls within a separation distance bin represented by Δ.

4. Evaluate the intra-event variability σ_ε^2 via regression residuals from step 1 or from the plateau of the semivariogram, assuming that for long separation distances, the following approximation is valid:

$$\frac{1}{2}\sigma_d^2(\Delta) \approx \sigma_\varepsilon^2 \quad (8)$$

5. Evaluate the distance-dependent correlation coefficient:

$$\rho_\varepsilon(\Delta) = 1 - \frac{\sigma_d^2(\Delta)}{2\sigma_\varepsilon^2} \quad (9)$$

The use of the sample semivariogram assumes stationarity and isotropy of the data [12].

4. Strong motion network, data and data processing

Istanbul Rapid Response and Early Warning System:

Istanbul is a mega-city which is exposed to high seismic hazard, located close to the Marmara Fault. The Marmara Fault is a part of the North Anatolian Fault, where a large earthquake of $M_w \geq 7$ occurring in the next 30 years is expected with a probability of more than 40% [9]. Particularly after the 1999 Izmit and Düzce Earthquakes, major efforts have been made to investigate the earthquake hazard and vulnerability in Istanbul. The IERREWS, a dense array of 100 strong motion recorders, has been established in the urban area for rapid response and early warning purposes. It provides information on ground shaking, damage and loss distributions within five minutes after an earthquake [14]. Figure 1 shows the distribution of these recording stations in the urban area of Istanbul. The relative spacing is about 2-3 km. The interstation distances vary between 0.67 km and 56 km. In 2012, 20 new instruments have been added. All stations consist of external, tri-axial (three orthogonal axes), force-balance (servo)-type accelerometers, recorders, and timing and communication modules [15].

The site conditions at individual recording sites have been investigated in several microzonation projects conducted by the Istanbul Metropolitan Municipality [16] and are available in terms of V_{S30}, displayed in Figure 2.

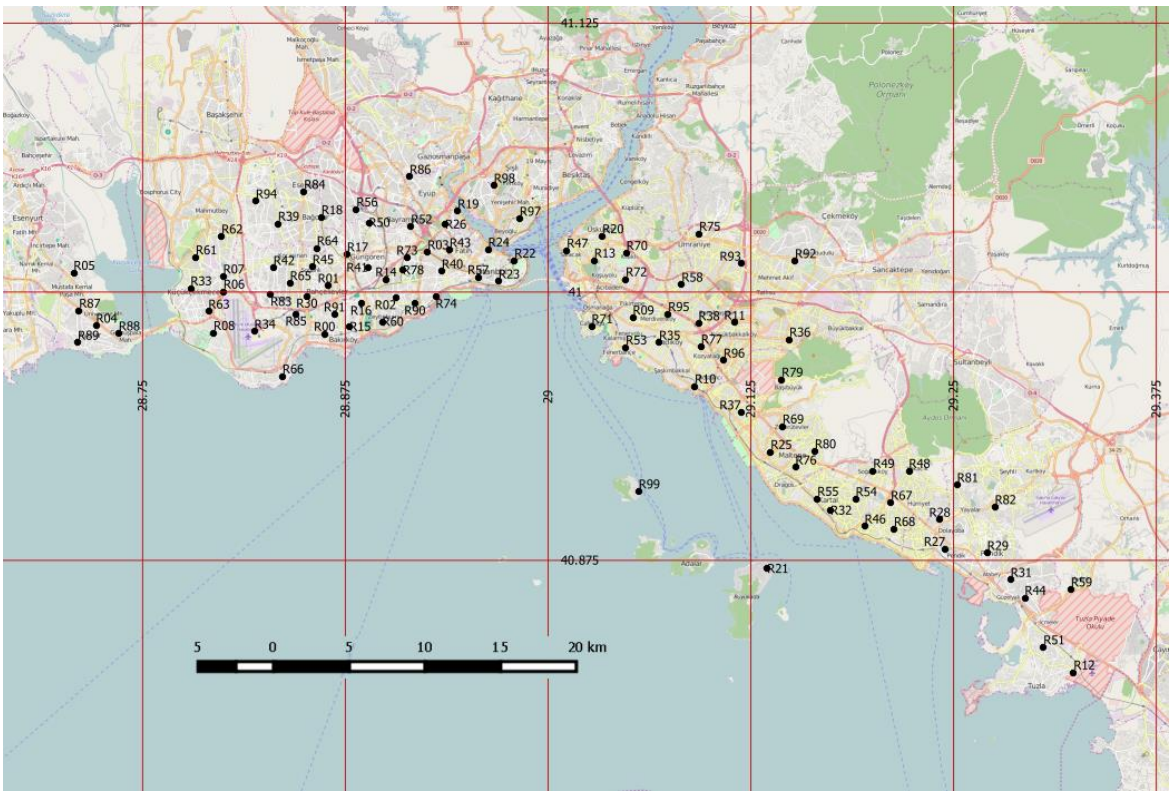

Figure 1. Location of the 100 rapid response stations that recorded the data used in this study.

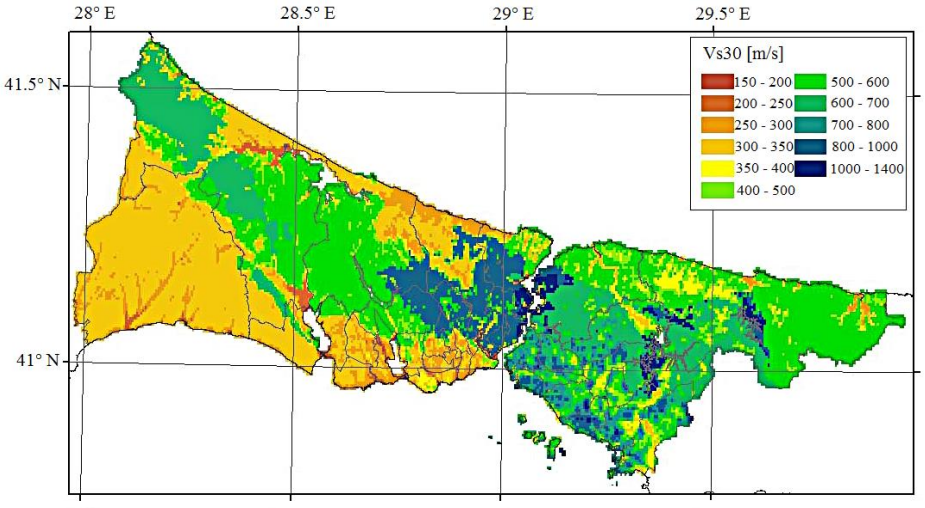

Figure 2. Average shear-wave velocity (V_{S30}) distribution. From Harmandar [17].

The dataset used in this study consists of 372 acceleration time histories recorded at the IERREWS, each with two horizontal components, from eight small-to-moderate events (M_w3.5 – M_w5.1) that occurred between 2003 and 2013 in the Marmara region. Table 1 summarizes the source

parameters. The M_w values of events 1-7 are taken from Kalafat [18], while the M_w value of event 8 is obtained from the GFZ GEOFON Program [19]. The focal depths vary between 10 and 17 km. The fault plane solutions are strike-slip mechanism for the first six events [20]. The fault mechanisms of events 7 and 8 are normal faulting [20] and oblique faulting (strike-slip and normal types, [19]), respectively. The epicenter locations are displayed in Figure 3. The magnitude-distance distribution is given in Figure 4.

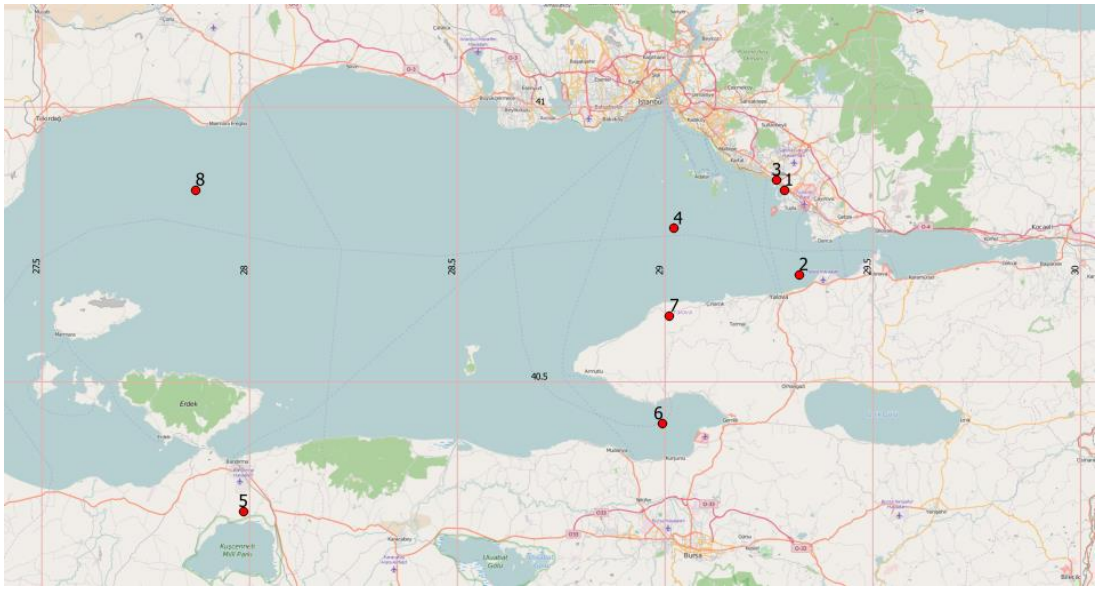

Figure 3. Epicenters of events 1-8.

Table 1. Source parameters of the earthquakes used in this study.

ID	Date	Longitude	Latitude	M_w	Depth [km]	Fault Mechanism	Number of Records
1	19/09/03	29.29	40.85	3.5	11.0	Strike Slip	16
2	16/05/04	29.32	40.70	4.3	10.0	Strike Slip	71
3	24/06/04	29.27	40.87	3.6	17.0	Strike Slip	13
4	29/09/04	29.02	40.78	4.1	13.0	Strike Slip	84
5	20/10/06	27.98	40.26	4.7	10.9	Strike Slip	42
6	24/10/06	28.99	40.42	5.1	12.5	Strike Slip	41
7	12/03/08	29.01	40.62	4.3	10.0	Normal Fault	54
8	27/11/13	27.87	40.85	4.8	10.8	Oblique	51

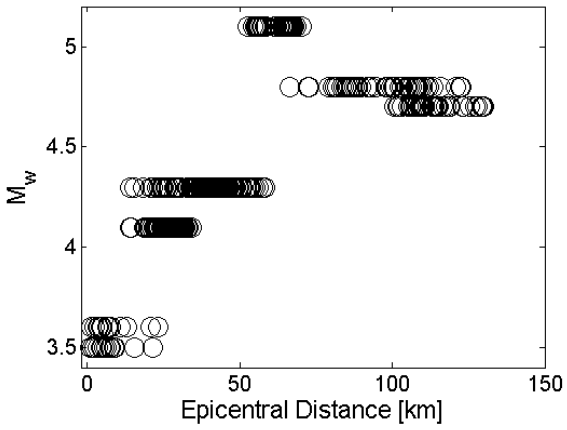

Figure 4. Magnitude-distance distribution of the IERREWS dataset.

The records are processed by performing the following steps:

1. Zero-order and first-order baseline correction.
2. Zero-pads are added to the beginning and the end of the record [21].
3. All records are bandpass-filtered with a fourth order Butterworth filter. The filter range is determined for each record individually by inspecting the spectral shape of the Fourier Amplitude Spectrum (FAS) of both horizontal components. The filter range is the same for both horizontal components. The low-cut filter is chosen observing the deviation from an omega-squared source model of the FAS [22]. The high-cut filter is applied where the spectrum deviates from a linear decay [22]. The low-cut corner frequency varies between 0.1 Hz and 2 Hz whereby over 90% of all selected low-cut frequencies are less than or equal to 0.5 Hz. The high-cut frequency varies between 20 Hz and 30 Hz.

5. Evaluation of intra-event spatial correlation

For the following analysis, we use the geometric mean of the horizontal components of PGA and 5%-damped PSA at 10 equally-spaced natural periods ranging from T_n = 0.1 s to T_n = 1.0 s. The primary selection criteria for candidate GMPEs considered for determining the intra-event residuals

are their suitability for an active tectonic region and the coverage of PGA and spectral values up to the natural period of 1.0 s, as this is used for the calculation of losses in Zeytinburnu (section 7 of this paper). Figure 5 shows the PGA data of events 2, 4, and 7 in comparison to the ground motion models by Kalkan and Gülkan [23], Özbey et al. [24], and Akkar and Bommer [10].

The model by Kalkan and Gülkan is based on 112 records from 57 events that occurred between 1976 and 2003 in Turkey. The model by Özbey et al. is based on 195 records (17 events) from Northwestern Turkey and therefore provides a regional ground motion model for Istanbul and the Marmara region. The model by Akkar and Bommer is based on 532 records (131 events) from Europe, the Mediterranean region and the Middle East.

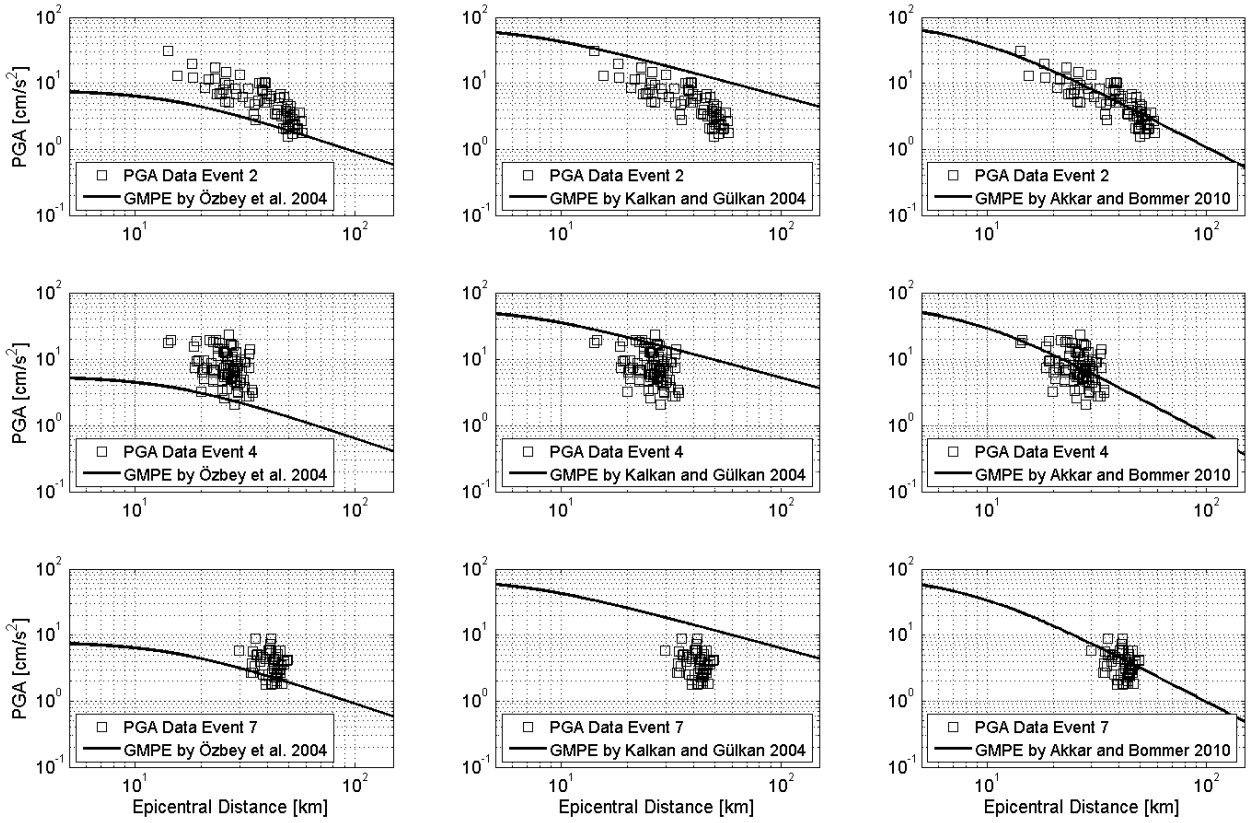

Figure 5. PGA data of event 2, 4, and 7 compared to the GMPEs by Kalkan and Gülkan (left), Özbey et al. (middle) and Akkar and Bommer (right).

The Akkar-Bommer GMPE provides a significantly better estimation of PGA compared to the two Turkish models, which consistently overestimate (Kalkan and Gülkan) or consistently underestimate (Özbey et. al) the observed ground motions. Additionally, we discover that the attenuation with epicentral distance of PGA of event 2 is predicted reasonably well by Akkar and Bommer (Figure 5a). Thus, we choose this GMPE for further examination. We test the trend of ε with regard to the two main explanatory variables R and V_{S30} (Figure 6). The PGA residuals are

unbiased in terms of R and V_{S30}. A minor trend of ε is observed in the PSA data (T_n=0.3 s) with regard to V_{S30} (Figure 7 d). It can be observed that this minor trend is also present in the PSA data at higher natural periods.

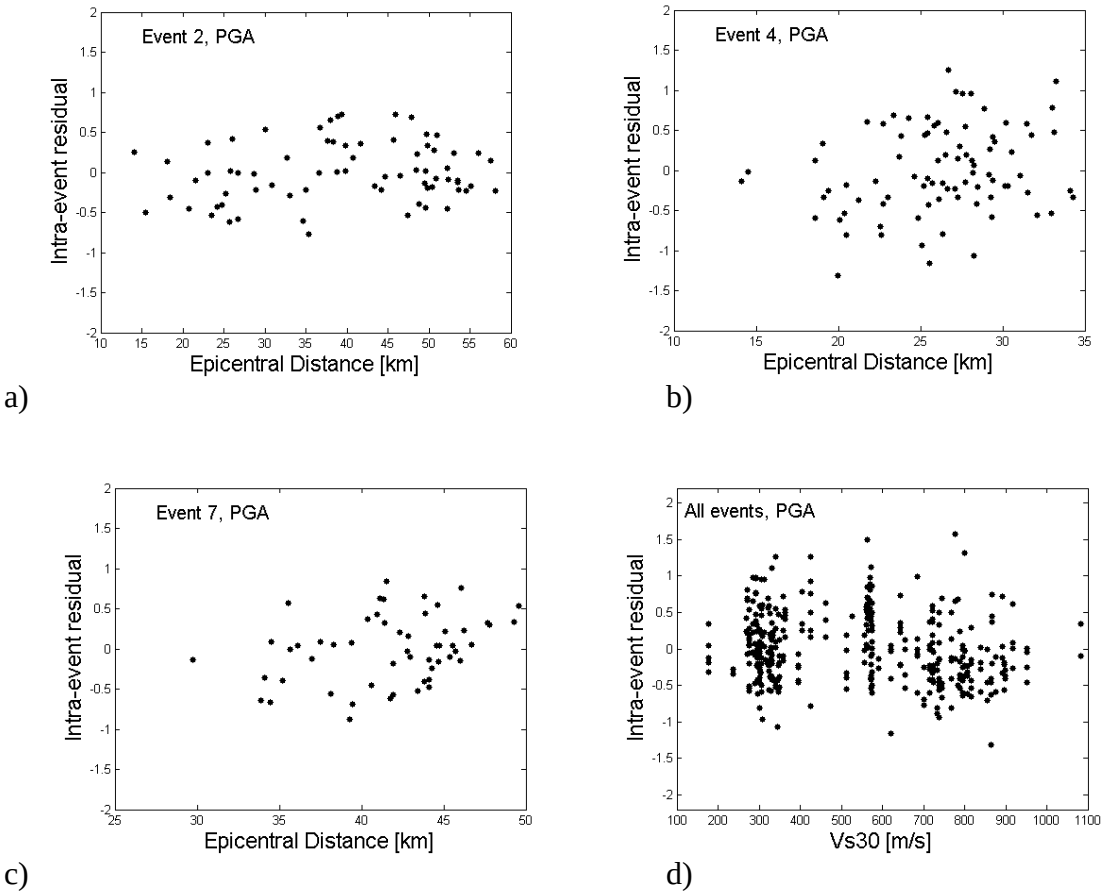

Figure 6. Intra-event residuals (PGA) computed with regard to the GMPE by Akkar and Bommer vs. epicentral distance of events 2, 4, and 7, and intra-event residuals vs. V_{S30} of all 8 events.

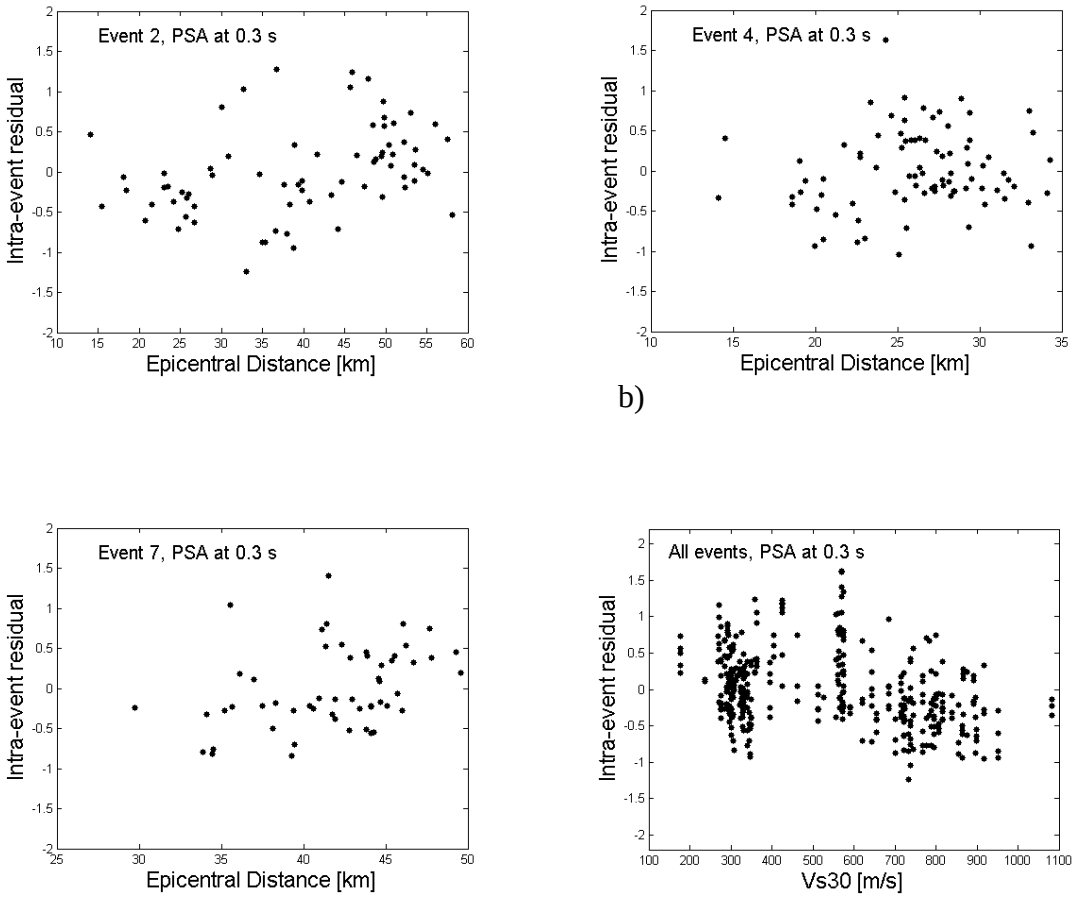

Figure 7. Intra-event residuals (PSA at 0.3 s) computed with regard to the GMPE by Akkar and Bommer vs. epicentral distance of events 2, 4, and 7, and intra-event residuals vs. V_{S30} of all 8 events.

In the following, we use the Akkar and Bommer GMPE as the basis of our analysis.
The functional form is

$$\log(GMP) = b_1 + b_2 M + b_3 M^2 + (b_4 + b_5 M)\log\sqrt{R^2 + b_6^2} + b_7 S_s + b_8 S_A + b_9 F_N + b_{10} F_R, \quad (10)$$

where S_s and S_A take the value of 1 for $V_{S30} < 360$ m/s and 360 m/s $\leq V_{S30} \leq$ 750 m/s, respectively, and zero otherwise. F_N and F_R take the value of 1 for normal and reverse faulting earthquakes, respectively, and zero otherwise. Note that in the original Akkar-Bommer model, R, denotes the Joyner-Boore distance in km, while in this study the epicentral distance is used due to the small-to-moderate magnitude range of M_w3.5 - M_w5.1, where point-source approximation is valid. Pairs of the intra-event residuals are then constructed for each of the 8 events. Subsequently, those pairs are assigned to bins according to their interstation distance Δ. In order to provide representative

averages in each bin, we choose 100 as the minimum number of data pairs per bin. To obtain this number of data pairs in the first bin (i.e. shortest interstation distance), the minimum bin-width of 1.4 km is used. At long interstation distances, this choice of bin-width creates the last bin containing at least 100 residual pairs at Δ = 39.9 km. The total number of bins up to this distance is 29. The number of ε-pairs per event is listed in Table 2. The total number of remaining residual pairs after the removal of bins corresponding to Δ > 39.9 km is 10,149. The histogram of the residuals data with regard to separation distance is presented in Figure 8.

Table 2. Number of residual pairs per event.

Event	1	2	3	4	5	6	7	8	All
Number of records	16	71	13	84	42	41	54	51	372
Number of residual pairs	120	2485	78	3486	861	820	1431	1275	10556
Number of used residual pairs	120	2416	78	3383	783	796	1414	1159	10149

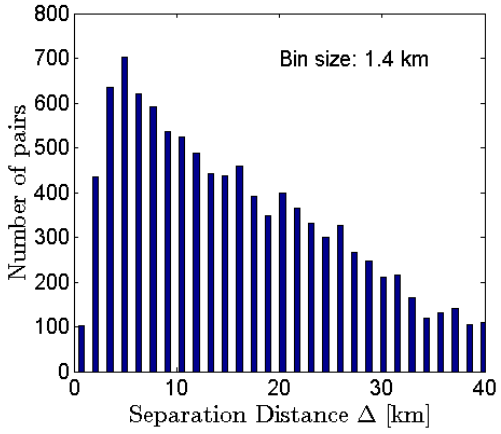

Figure 8. Number of residual pairs per bin. Minimum number of pairs per bin is 100. All bins corresponding to Δ > 39.9 km are not considered since the amount of datapairs per bin is less than 100.

5.1 Results for PGA

For each bin, we evaluate the variance of the pairwise differences of intra-event residuals $\sigma_d^2(\Delta)$ and the semivariogram as introduced in equation (7). The semivariogram (Figure 9 left) of the PGA residuals shows increasing variability with increasing separation distance. The expected plateau can be identified between 20 km and 40 km separation distance, indicating that $\sigma_\varepsilon^2 \approx 0.25$, while the direct evaluation of the residual variance is $\sigma_\varepsilon^2 = 0.21$. We evaluate $\rho_\varepsilon(\Delta)$ according to equation (9)

by using the σ_ε^2-estimate from the semivariogram plateau and develop an empirical relationship of the functional form $\rho_\varepsilon(\Delta) = \exp(-\alpha\Delta^\beta)$ based on the nonlinear least squares method (Figure 9 right). The correlation curve shows a rapid decay with increasing Δ, with a correlation length of Δ_c = 3.5 km (the distance for which ρ_ε decreases to 1/e).

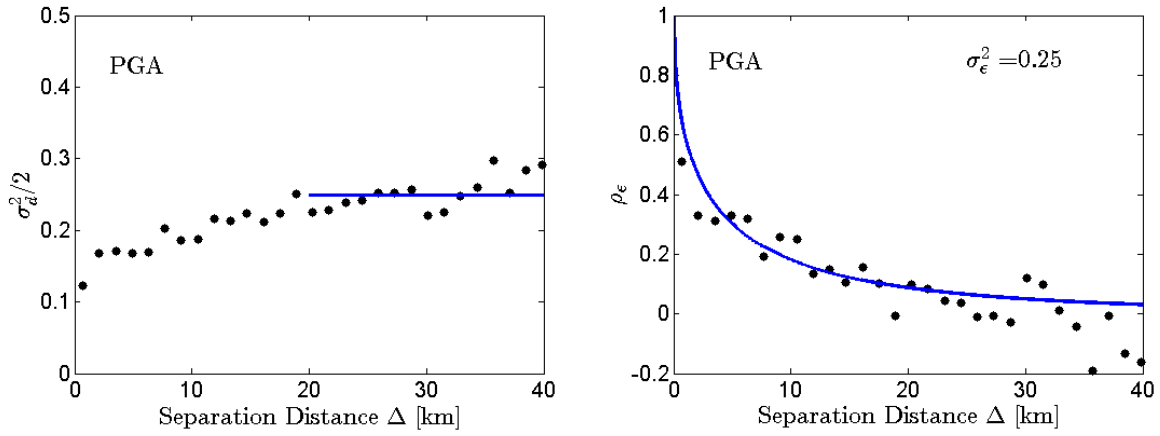

Figure 9. Left side: Semivariogram (PGA). An increase with separation distance is observed, forming a plateau of approximately 0.25 at 20 km < Δ < 40 km, which is comparable to σ_ε^2 computed from the residual variance (0.21). Right side: Correlation coefficient versus Δ with fitted exponential model $\rho_\varepsilon(\Delta)$=exp(-0.5272$\Delta^{0.5112}$). σ_ε^2=0.25 is determined from the semivariogram at 20 km < Δ < 40 km. The correlation length is 3.5 km.

5.2 Results for PSA

To investigate the spatial correlation of PSA, the same procedure as for PGA is applied. Again, we calculate the intra-event residuals with respect to the Akkar-Bommer GMPE for natural periods up to 1.0 s and evaluate the semivariograms for interstation distances up to 40 km.

The intra-event variability σ_ε^2 is then estimated by identifying a constant portion in the semivariograms at large Δ and compared with the residual variances. The expected plateaus at long distances can be identified at all natural periods, although in some cases, a deviation from the expected shape is observed, i.e. at Δ = 40 km for T_n = 0.7 s (Figure 11 left). As observed for PGA, the σ_ε^2 values estimated from the semivariogram plateaus are larger than the residual variances for all natural periods. Due to the dense station spacing in Istanbul and the small area of investigation, the influence of correlated residuals on the sampling variance is likely to be the reason for the observed gap between the two σ_ε^2 estimates [4,25]. Apart from PSA at 0.1 s, the difference between the two

estimates is less than or equal to 0.04.

Table 3. Comparison of the σ_ε^2 values derived from the residual variances and the semivariogram plateau.

Period [s]	σ_ε^2 (semivariogram)	Var(ε)
0 (PGA)	0.25	0.21
0.1	0.35	0.26
0.2	0.33	0.29
0.3	0.29	0.26
0.4	0.25	0.23
0.5	0.25	0.24
0.6	0.27	0.25
0.7	0.26	0.23
0.8	0.25	0.22
0.9	0.25	0.21
1.0	0.25	0.21

The correlation coefficients $\rho_\varepsilon(\Delta)$ of PSA are evaluated by using the σ_ε^2 values from the semivariogram plateaus. The same functional form as for the PGA is chosen to fit an empirical model to $\rho_\varepsilon(\Delta)$. Three selected plots (T_n = 0.3 s, 0.7 s, and 1.0 s) are presented in Figures 10-12 (semivariogram on the left side, while correlation coefficient with the fitted exponential model on the right side). For all natural periods, increasing variability of PSA and therefore decreasing correlation are observed. Table 4 lists the model coefficients and the resulting correlation lengths. We emphasize that the shortest interstation-distance in the IERREWS is 0.67 km and that interstation-distances below 1 km are underrepresented in the dataset. At short separation distances (less than 1 km), wherein empirical data are limited and estimates are uncertain, discretion is required in adopting such models for seismic hazard and risk assessment of spatially distributed structures. However, correlation coefficients at separation distances around 1 km are well constrained in our dataset, which makes our model unique in terms of resolution compared to the datasets used for spatial correlation models in the literature. Due to the condition that ρ_ε at Δ = 0 km is fixed at 1.0, correlation models in the literature provide values for ρ_ε at short distances (e.g. Δ < 2 km) independent from the smallest statistically significant station separation bin. We state that in our case the correlation at this distance represents a measured quantity.

Comparing the fitted correlation models for PGA and PSA at different periods indicates that the models for PGA and PSA at periods up to 0.5 s show no significant variation (Figure 13). The correlation lengths vary between 2.5 km and 3.8 km. However, for larger T_n, the model exhibits an

increasing trend of Δ_c with the natural period, which is clearly visible in the right plot of Figure 13. The corresponding correlation lengths increase from 2.5 km (T_n = 0.2 s) to 8.5 km (T_n = 1.0 s).

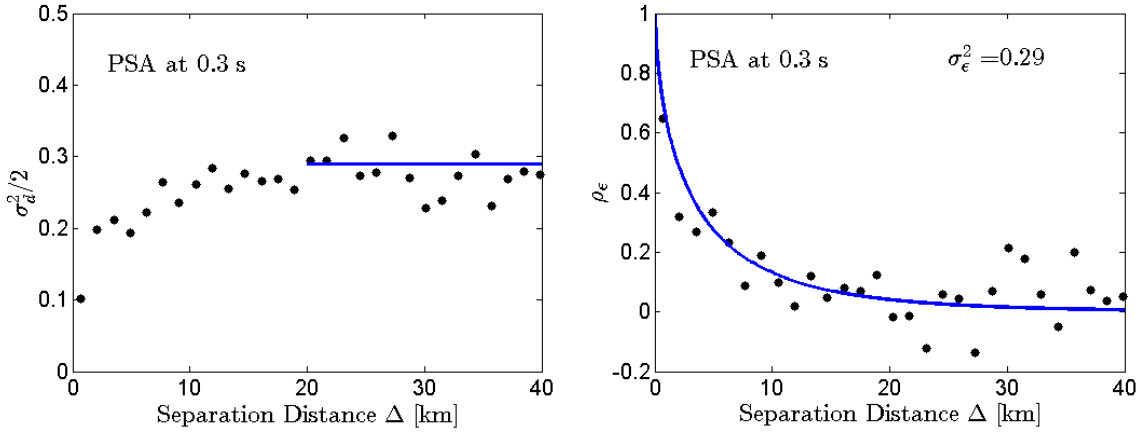

Figure 10. Semivariogram (left side) and $\rho_\varepsilon(\Delta)$ with fitted exponential model (right side) for PSA at T_n = 0.3 s. σ_ε^2 = 0.29 is estimated by visual inspection of the semivariogram-plateau, indicated by the blue line. The correlation length is 3.4 km.

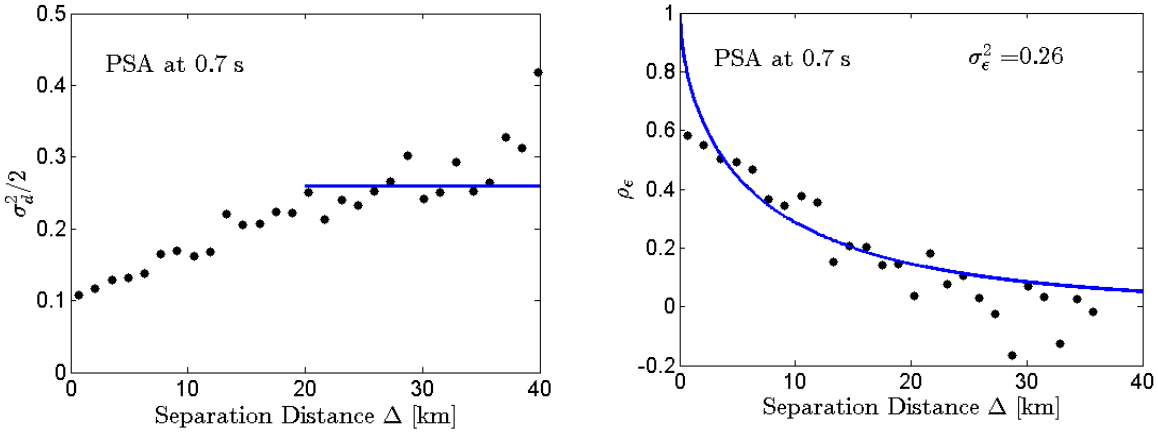

Figure 11. Semivariogram (left side) and $\rho_\varepsilon(\Delta)$ with fitted exponential model (right side) for PSA at T_n = 0.7s. σ_ε^2 = 0.26 is estimated by visual inspection of the semivariogram-plateau, indicated by the blue line. The correlation length is 6.9 km.

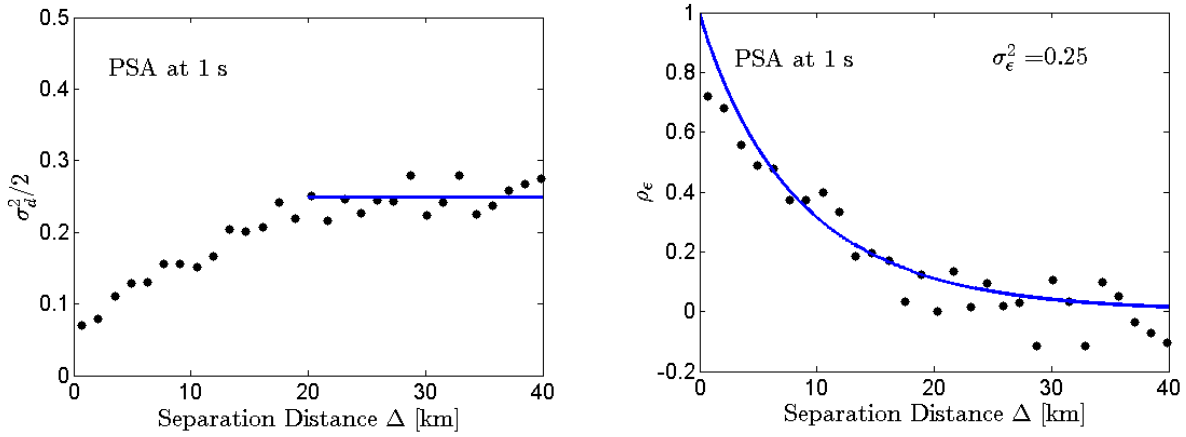

Figure 12. Semivariogram (left side) and $\rho_\varepsilon(\Delta)$ with fitted exponential model (right side) for PSA at T_n = 1.0 s. σ_ε^2 = 0.25 is estimated by visual inspection of the semivariogram-plateau, indicated by the blue line. The correlation length is 8.5 km.

Table 4. Coefficients and correlation lengths Δ_c of the exponentially decaying spatial correlation model $\rho_\varepsilon(\Delta)=\exp(-\alpha\,\Delta^\beta)$ for PGA and PSA at periods from 0.1 s - 1.0 s.

Period [s]	α	β	Δ_c [km]
0.0 (PGA)	0.5272	0.5112	3.5
0.1	0.6433	0.3986	3.0
0.2	0.6462	0.4808	2.5
0.3	0.4515	0.6537	3.4
0.4	0.5060	0.6324	3.0
0.5	0.4437	0.6032	3.8
0.6	0.2990	0.6412	6.6
0.7	0.3014	0.6189	6.9
0.8	0.1856	0.8605	7.0
0.9	0.1351	0.9603	8.0
1.0	0.1374	0.9257	8.5

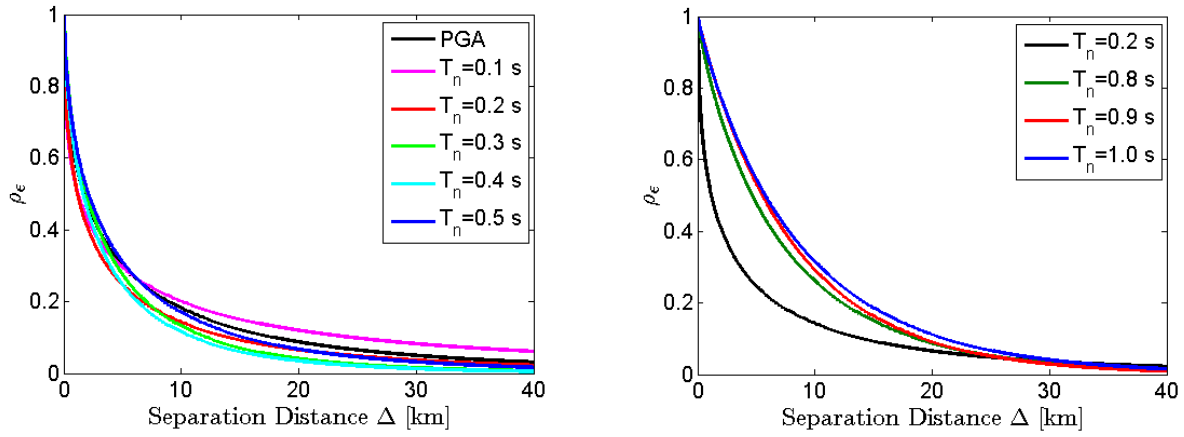

Figure 13. Comparison of the fitted models for different natural periods. Left: PGA and short-period PSA up to 0.5 s. No significant differences are observed. The correlation lengths are in the range of 2.5 km - 3.8 km. Right: The correlation models for PSA at periods longer than 0.5 s exhibit notably longer correlation lengths of typically 7-8 km.

6. Comparison with other intra-event correlation models

Several studies have developed intra-event spatial correlation models of ground motion parameters. The areas of investigation include Japan [3,5,12,13], California [4,26,27], Taiwan [3,11], and Europe [6,28]. Among these models, there are notable differences in terms of the characteristics of the underlying datasets and the procedures applied to calculate spatial correlations. In some cases, records of a single event are used; other studies analyze a combined set of multiple events. For this reason, the size of the datasets varies between 230 records [3] and 6224 records [5]. In the majority of the studies, equation (4) is used to determine $\rho_\varepsilon(\Delta)$ based on the sample semivariogram, whereas other studies directly evaluate the normalized covariance [3,11].

Moreover, the distance range per bin varies from less than 1 km (e.g. Boore et al. [26] grouped the data into bins such that 15 station pairs fall within a bin) to 5 km and more [6]. The largest separation distance varies between 10 km and over 100 km. The majority of investigations consider PGA and PSA at different periods, whereas some studies analyze PGA or PGV only. Apart from that, the choice of the component of recorded ground motion varies (i.e. randomly orientated horizontal component, larger horizontal component, or geometric mean of both horizontal components).

The estimation of the intra-event variability σ_ε^2 is carried out in different ways. Goda and Atkinson

[5] inspected the semivariogram-plateaus for each event individually and normalize each residual subsequently with the intra-event variability of the corresponding event. Wang and Takada [3] determined σ_ε^2 from the variance of the intra-event residuals with respect to the chosen GMPE. In other studies, a regression analysis was performed to obtain a suitable GMPE for the dataset to be analyzed, and then σ_ε^2 is obtained from the regression residuals [4,11].

In contrast to this study, all the examples listed above are (predominantly or entirely) based on events of $M_w \geq 5$.

In Figure 14 (left), the PGA-correlation model from this study is compared to selected models reported in the literature.

1. Japan:
   - Wang and Takada [3] is based on records of the 2004 Mid-Niigata (M_w6.6) event.
   - Goda and Atkinson [5] is derived from 20 Japanese events (6224 records, M_w5.6 - 6.8).
2. Taiwan:
   - Goda and Hong [4] is based on the 1999 Chi-Chi (M_w7.6) records.
3. California:
   - Boore et al. [26] is based on the 1994 Northridge (M_w6.7) records.
   - Goda and Hong [4] is based on 375 records of 6 events that occurred between 1979 and 1999 (M_w6.0 - 7.1).

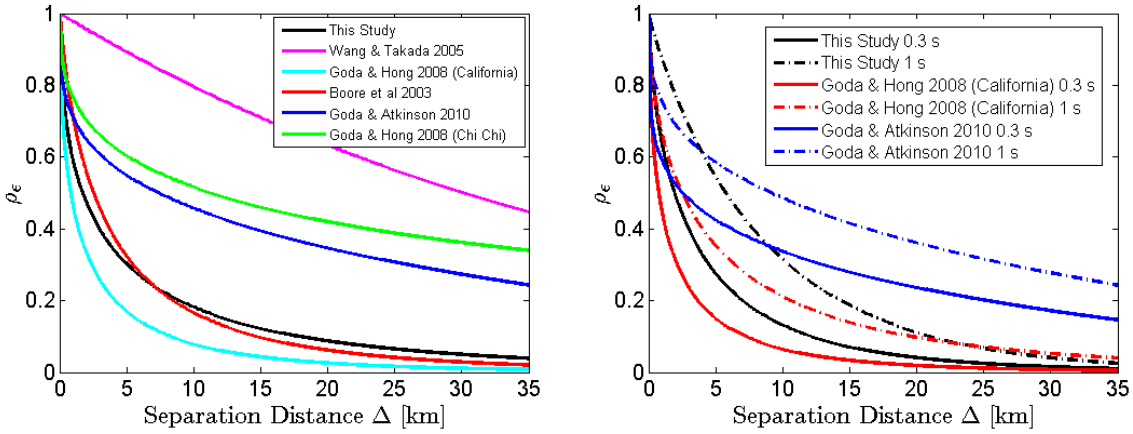

Figure 14. Correlation model of this study compared to different correlation models reported in the literature (PGA on the left side, PSA with T_n=0.3 s and 1.0 s on the right side). Large variability in the correlation lengths is observed (1.65 km to 43.5 km). Correlation models based on Japanese and Taiwanese data generally exhibit a more gradual decay with distance and longer correlation lengths compared to our model and the California model. The period dependence of the

PSA correlation coefficient (more gradual decay with distance for longer periods) was observed by Goda and Hong [4] in California as well as by Goda and Atkinson [5] in Japan.

The curves in Figure 14 (left) show that the correlation lengths vary significantly among different studies from 1.65 km to 43.5 km. Crowley et al. [1] mentioned that the extreme long correlation lengths in Wang and Takada [3] are 'heavily influenced by regional factors, such as wave propagation, site conditions and perhaps the fault rupture mechanism'. Generally, it is observed that Japanese and Taiwanese models decrease more gradually and consequently have much longer correlation lengths than those determined in this paper. The results based on records from California, however, are comparable to those from Istanbul, specifically the Boore et al. [26] model. Figure 14 (right) compares the results of this paper with the PSA-correlation at T_n = 0.3 s and 1.0 s from Goda and Hong [4] (California) and Goda and Atkinson [5] (Japan). It is clear that the correlation lengths of PSA derived from Japanese data are notably longer than those from Istanbul and California. The period dependency of the correlation coefficient (more gradual decay with distance for longer periods) is observed in all of the three studies.

7. Impact on loss assessment – case study for Zeytinburnu

To study the effect of the established intra-event correlation model on earthquake loss estimation, we simulate a M_w7.2 scenario earthquake on the Marmara Fault with epicenter 28.84E° and 40.9N° and generate ground motion fields (PGA and PSA at T_n = 0.3 s and 1.0 s) in the district Zeytinburnu on the European side of Istanbul (located at a distance of about 12 km from the simulated fault trace). We apply the Monte Carlo method to investigate the probability distribution of aggregated economic loss. The area of Zeytinburnu (~12km^2) is subdivided into 52 geocells, each of which is bounded by 0.005 degrees of longitude and latitude, which corresponds to approximately 0.426 km and 0.556 km in EW and NS direction, respectively. The portfolio consists of 11,250 reinforced concrete (T_y = ~0.18-0.85 s) and masonry (T_y = ~0.11-0.46 s) buildings (1-9 stories), that are assigned to five aggregated building classes according to HAZUS [29]. The total replacement value of the portfolio is 2.406 billion EUR. For damage and loss calculations, we use the MATLAB-based software SELENA [31], which applies the capacity spectrum method to determine the probability of structural failure in five damage classes. Based on the damage class, mean damage ratio and aggregated economic loss in EUR are calculated including demolition costs. Further details regarding the scenario, SELENA, HAZUS, the Turkish damage ratio assumptions and the properties of the pre-code Zeytinburnu building stock can be found in Daniell [29,30].

In SELENA, demand spectra are based on PGA and the spectral ordinates at 0.3 s and 1.0 s. In order to generate correlated response spectra, the correlation between different ground motion parameters (e.g. PGA and PSA at T_n = 0.3 s) needs to be considered [1]. We define $\rho_\varepsilon(\Delta,T_{n1},T_{n2})$ as the intra-event correlation coefficient of PSA at two natural periods T_{n1} and T_{n2}, where PSA at T_n = 0.0 s represents PGA. We use the approximation [4,32]

$$\rho_\varepsilon(\Delta,T_{n1},T_{n2}) \approx \rho_0(T_{n1},T_{n2})\,\rho_\varepsilon(\Delta,T_{max},T_{max}) \quad (11),$$

where $\rho_0(T_{n1},T_{n2})$ represents the correlation coefficient of PSA at two natural periods T_{n1} and T_{n2} at the same site (Δ = 0), and T_{max} denotes the larger value of T_{n1} and T_{n2}. We use the 372 intra-event residuals of PGA and PSA at T_n = 0.3 s and 1.0 s from our dataset and evaluate ρ_0 (0.0 s,0.3 s) ≈ 0.71, ρ_0(0.0 s,1.0 s) ≈ 0.28, and ρ_0(0.3 s,1.0 s) ≈ 0.44 (Figure 15). The following method in the simulation of ground motion fields is applied. First, the medians of the logarithms of PGA and PSA at T_n = 0.3 s and 1.0 s are calculated for each geocell by using the GMPE by Özbey et al. Subsequently, a 156×156 covariance matrix is constructed (i.e. 3 ground motion parameters for 52 geocells), where each element is given by

$$COV(\Delta,T_{n1},T_{n2}) = \rho_\varepsilon(\Delta,T_{n1},T_{n2})\,\sigma_\varepsilon(T_{n1})\,\sigma_\varepsilon(T_{n2}) \quad (12).$$

$\rho_\varepsilon(\Delta,T_{n1},T_{n2})$ is calculated by using equation (11) and Δ represents the distance between the reference points of the geocells. A vector of correlated residuals ε can then be generated and added to the median ground motion term in order to obtain a realization of spatially correlated ground motion parameters [8,29].

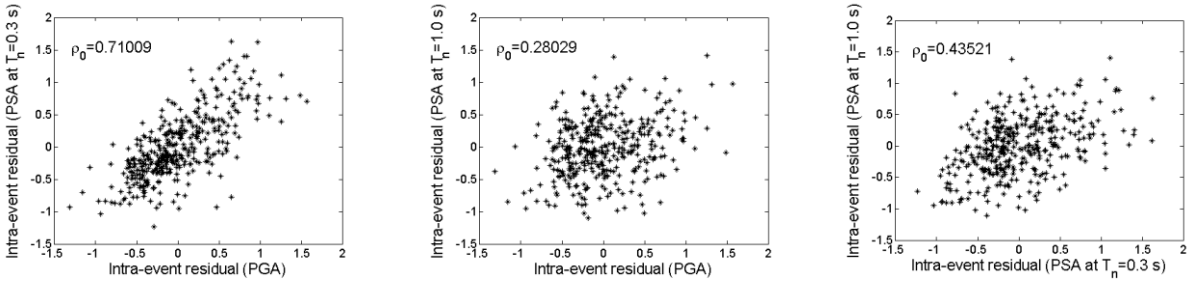

Figure 15. Scatter plots of intra-event residuals $\varepsilon(T_{n1})$ and $\varepsilon(T_{n2})$ for T_n=0 s (PGA), 0.3 s and 1.0 s. The correlation coefficients are evaluated as ρ_0(0.0 s,0.3 s) ≈ 0.71, ρ_0(0.0 s,1.0 s) ≈ 0.28, and ρ_0(0.3 s,1.0 s) ≈ 0.44.

We implement 8 different $\rho_{\varepsilon}(\Delta)$ models in order to investigate their effects on the probability distribution of economic loss. For each $\rho_{\varepsilon}(\Delta)$ model, 800 realizations of ground motion are generated. The shake maps shown in Figure 16 illustrate the effects of the different correlation models on the spatial distribution of PGA. The loss histograms of three selected cases are shown in Figure 17 with the distribution parameters, mean μ, median m, standard deviation σ, and skewness S. Due to the uniformly modeled ground motion within each geocell (i.e. full correlation within each geocell), it can be expected that there is overcorrelation within our calculations which might marginally affect the loss distributions in an upward direction. Table 5 gives an overview of the chosen correlation models with the corresponding correlation lengths and the loss estimation results in terms of distribution parameters. Uncorrelated ground motion results in a narrow, bell-shaped loss distribution with a mean of 1.62 billion € and a coefficient of variation (C_V) of 0.108. When our correlation model is implemented, the mean loss remains unaltered but the shape of the loss distribution changes significantly (Figure 17b). The coefficient of variation increases to 0.384 and the loss distribution is skewed towards higher losses. The included spatial correlation increases the likelihood of simultaneous large ground motions in many geocells, as illustrated in the realizations of simulated PGA-distributions in Figures 16b and 16c. Consequently, the likelihood of simultaneous damage of many buildings increases. The Californian model by Goda and Hong [4] provides specific correlation curves for PGA and PSA at T_n = 0.3 s and 1.0 s and therefore, enables a direct comparison to our model. The calculated values of mean and median of the loss distribution are similar to the ones based on the correlation model of this study; C_V, however, is only 0.324, probably due to the smaller correlation, especially for short site-to-site-distances (Figure 14), which is crucial for a test area of the size of Zeytinburnu. Additionally, we observe higher variability in the loss distributions when increasing the correlation length in a simple single-parameter exponential model as proposed in Wang and Takada [3], approaching the case of perfect correlation (C_V = 0.479).

Table 5. Different correlation models compared in our case study with the corresponding correlation lengths and the results in terms of distribution parameters of economic loss.

Correlation Model	Δ_c [km]	Mean [10^9 EUR]	Median [10^9 EUR]	Standard deviation [10^9 EUR]	Skewness
Uncorrelated	0	1.616	1.612	0.175	-0.115
This Study	3.4 - 8.5	1.626	1.687	0.624	-0.468
Goda and Hong 2008	1.5 - 4.7	1.622	1.700	0.526	-0.502
Boore et al. 2003	4.18	1.597	1.687	0.578	-0.453
exp([-Δ/Δ_c])	8	1.660	1.783	0.642	-0.540
exp([-Δ/Δ_c])	10	1.657	1.780	0.663	-0.519
exp([-Δ/Δ_c])	30	1.631	1.740	0.681	-0.490
Full Correlation	∞	1.573	1.697	0.735	-0.345

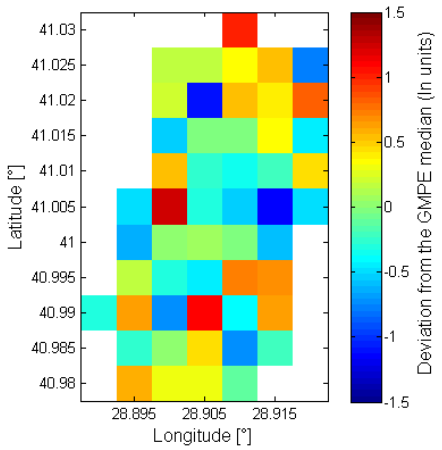

a)

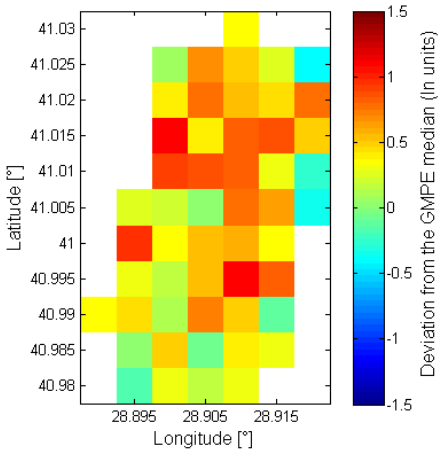

b)

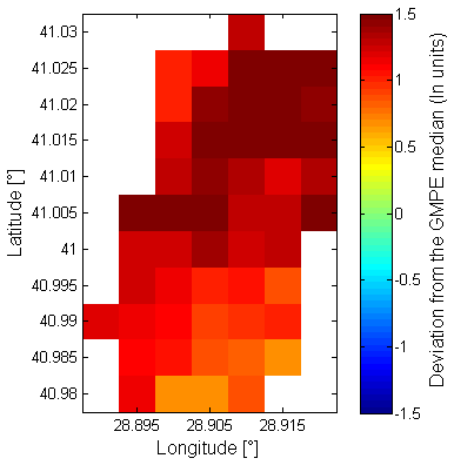

c)

Figure 16. Realizations of simulated PGA-distribution in Zeytinburnu with various correlation properties: no spatial correlation (a), correlation model as derived in this study (b), simple one-parameter exponential decay with 10 km correlation length (c). The maps display the difference to the predicted median in the Özbey et al. [24] GMPE for each geocell.

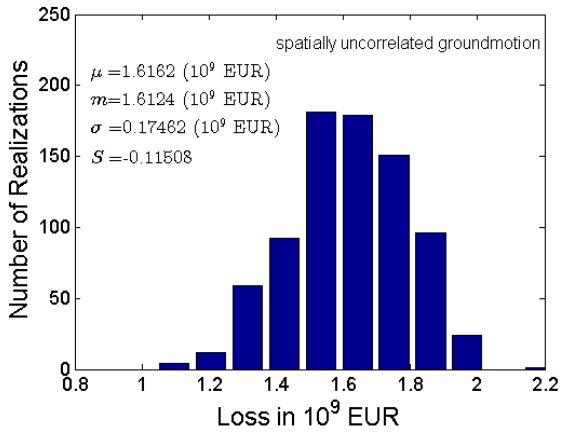

a)

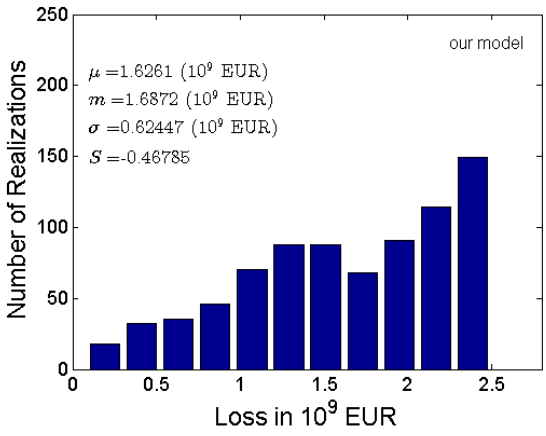

b)

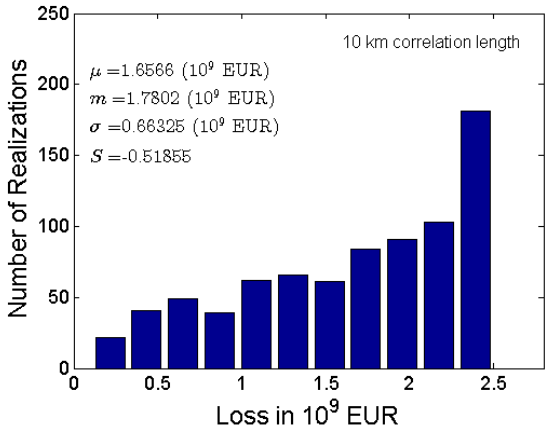

c)

Figure 17. Histograms of aggregated economic loss in Zeytinburnu resulting from different spatial correlation models. a) uncorrelated ground motion b) period dependent correlation model as established in this study c) $\rho_{\varepsilon}(\Delta)$ = exp(-[1/10 km] Δ) for PGA and PSA of all natural periods. While the mean loss remains essentially unaltered, the coefficient of variation increases with increasing correlation from 0.108 to 0.400.

8. Conclusions

We studied ground motion correlation properties in the Istanbul area for PGA and PSA values between 0.1 s and 1.0 s using accelerometric recordings of the Istanbul Rapid Response and Early Warning System (IERREWS) of 8 earthquakes with magnitudes between M_w3.5 and M_w5.1. During the 15 years of operation, no large events have been recorded by the IERREWS. The typical station spacing of 2 km within the IERREWS allows constraining the correlation properties with semivariograms for small distances. When we determined the correlation lengths from a functional form matched to the empirical correlation, we found correlation lengths of 2.5 to 4 km for PGA and PSA at $T_n \leq 0.5$ s. For larger natural periods up to 1.0 s, the correlation length is about 7 to 8 km. We compared these findings to other spatial correlation models from Japan, California and Taiwan, which are based on larger events. We observed a large regional dependence (e.g. significant differences in correlation lengths). The correlation properties found in California are similar to our results, whereas correlation models from Japan and Taiwan decay more gradually. On this basis and due to the lack of data from large events in the Istanbul area, we incorporated our model in a simulation of financial losses for a hypothetical building stock in Zeytinburnu due to a large M_w7.2 earthquake in the Marmara Sea. We demonstrated the relevance of the correlation length for seismic loss estimation by simulating 800 ground motion realizations for several correlation models and by

establishing the corresponding loss distribution.

In case of no correlation, a narrow bell-shaped distribution was found with a mean value of 1.62 billion € and a coefficient of variation of 11%. In this case the median loss was almost identical to the mean loss as the distribution was symmetric. Using full correlation resulted in a distribution with a slightly smaller mean value, a larger standard deviation, a higher median loss (1.70 billion €), and skewed towards higher losses. The correlation lengths found for Istanbul (3.5 to 8.5 km) resulted in a similar mean loss, a coefficient of variation of 38%, a median loss of 1.69 billion €, and a distribution skewed towards higher losses.

Thus for a scenario earthquake with only intra-event ground motion variability and the building portfolio in Zeytinburnu, increasing correlation lengths correspond to increasing losses reflected in increasing median loss and coefficient of variation. If the correlation lengths increase with the spectral period, as is the case in Istanbul, mid- and high-rise buildings will be more affected by correlation properties than low-rise buildings.

Since our model is based on events of $M_w \leq 5.1$, further analysis is required in the future with regard to potential magnitude dependence of spatial correlation properties and to test the sensitivity in loss estimations to different spatial correlation models.

List of Figures

Figure 8 Number of residual pairs per bin. Minimum number of pairs perbin is 100. All bins corresponding to Δ > 39.9 km are not considered since the amount of datapairs per bin is less than 100.

Figure 9 Left side: Semivariogram (PGA). An increase with separation distance is observed, forming a plateau of approximately 0.25 at 20 km < Δ < 40 km, which is comparable to σ_ε^2 computed from the residual variance (0.21). Right side: Correlation coefficient versus Δ with fitted exponential model $\rho_\varepsilon(\Delta)$=exp(-0.5272$\Delta^{0.5112}$). σ_ε^2=0.25 is determined from the semivariogram at 20 km < Δ < 40 km. The correlation length is 3.5 km.

Figure 10 Semivariogram (left side) and $\rho_\varepsilon(\Delta)$ with fitted exponential model (right side) for PSA at T_n = 0.3 s. σ_ε^2 = 0.29 is estimated by visual inspection of the semivariogram-plateau, indicated by the blue line. The correlation length is 3.4 km.

Figure 11 Semivariogram (left side) and $\rho_\varepsilon(\Delta)$ with fitted exponential model (right side) for PSA at T_n = 0.7s. σ_ε^2 = 0.26 is estimated by visual inspection of the semivariogram-plateau, indicated by the blue line. The correlation length is 7.5 km.

Figure 12 Semivariogram (left side) and $\rho_\varepsilon(\Delta)$ with fitted exponential model (right side) for PSA at T_n = 1.0 s. σ_ε^2 = 0.25 is estimated by visual inspection of the semivariogram-plateau, indicated by the blue line. The correlation length is 8.5 km.

Figure 13 Comparison of the fitted models for different natural periods. Left: PGA and short-period PSA up to 0.5 s. No significant differences are observed. The correlation lengths are in the range of 2.5 km - 3.8 km. Right: The correlation models for PSA at periods longer than 0.5 s exhibit notably longer correlation lengths of typically 7-8 km.

Figure 14 Correlation model of this study compared to different correlation models reported in the literature (PGA on the left side, PSA (T_n=0.3 s and 1.0 s) on the right side. Large variability in the correlation lengths is observed (1.65 km to 43.5 km). Correlation models based on Japanese and Taiwanese data generally propose a more gradual decay with distance and longer correlation lengths compared to California and to our model. The period dependence of the PSA correlation coefficient (more gradual decay with distance for longer periods) was observed by Goda and Hong [4] in California as well as by Goda and Atkinson [5] in Japan.

Figure 15 Scatter plots of intra-event residuals $\varepsilon(T_{n1})$ and $\varepsilon(T_{n2})$ for T_n=0 s (PGA), 0.3 s and 1.0 s. The correlation coefficients are evaluated as ρ_0(0.0 s,0.3 s) ≈ 0.71, ρ_0(0.0 s,1.0 s) ≈ 0.28, and ρ_0(0.3 s,1.0 s) ≈ 0.44.

List of Tables

Acknowledgements

We are indebted to Alexander von Humboldt Foundation who granted an AvH scholarship to K. Goda, which allowed him to supervise T. Wagener's MSc thesis on ground motion correlation. The Center of Disaster Management and Risk Reduction Technology (CEDIM) of KIT supported the work on the paper. We are grateful for valuable comments of Gail Atkinson and an anonymous reviewer; both helped to improve the manuscript.

References

[1] Crowley H, Stafford PJ, Bommer JJ. Can earthquake loss models be validated using field observations? Journal of Earthquake Engineering. 2008; 12(7): 1078-1104.

[2] Sokolov V, Wenzel F. Influence of spatial correlation of strong motion on uncertainty in earthquake loss estimation. Earthq Eng Struct Dyn. 2011; 40: 993–1009.

[3] Wang M, Takada T. Macrospatial correlation model of seismic ground motions. Earthquake Spectra. 2005; 21(4): 1137–1156.

[4] Goda K, Hong HP. Spatial correlation of peak ground motions and response spectra. Bull Seismol Soc Am. 2008; 98(1): 354–365.

[5] Goda K, Atkinson G. Intraevent spatial correlation of ground-motion parameters using sk-net data. Bull Seismol Soc Am. 2010; 100(6): 3055–3067.

[6] Cimellaro GP, De Stefano A, Reinhorn AM. Intra-event spatial correlation of ground motion using L´Aquila earthquake ground motion data. III ECCOMAS Thematic Conference on Computational Methods in Structural Dynamics and Earthquake Engineering; 2011.

[7] Goda K, Hong HP. Estimation of seismic loss for spatially distributed buildings. Earthquake Spectra. 2008; 24(4): 889–910.

[8] Park J, Bazurro P, Baker JW. Modeling spatial correlation of ground motion intensity measures for regional seismic hazard and portfolio loss estimation. Tenth International Conference on Application of Statistic and Probability in Civil Engineering (ICASP10), Tokyo, Japan, 2007, 8pp.

[9] Erdik M, Durukal E. Earthquake risk and its mitigation in Istanbul. Natural Hazards. 2008; 44: 181–197.

[10] Akkar S, Bommer JJ. Empirical equations for the prediction of PGA, PGV and spectral accelerations in Europe, the Mediterranean and the Middle East. Seismol Res Lett. 2010; 81:195–206.

[11] Sokolov V, Wenzel F, Jean WY, Wen KL. Uncertainty and spatial correlation of earthquake ground motion in Taiwan. Terrestrial, Atmospheric and Oceanic Sciences. 2010; 21(6): 905–921.

[12] Goda K, Atkinson G. Probabilistic characterization of spatially correlated response spectra f or earthquakes in Japan. Bull Seismol Soc Am. 2009; 99(5): 3003–3020.

[13] Goda K. Interevent variability of spatial correlation of peak ground motions and response spectra. Bull Seismol Soc Am. 2011; 101(5): 2522–2531.

[14] Sesetyan K, Zulfikar C, Demircioğlu M, Hancilar U, Kamer Y, Erdik M. Istanbul Earthquake Rapid Response System: Methods and practices. Soil Dyn Earthq Eng. 2011; 31: 170–180.

[15] Erdik M, Fahjan Y, Ozel O, Alcik H, Mert A, Gul M. Istanbul earthquake rapid response and early warning system, Bull. Earthq. Eng. 2003; 1: 157–163.

[16] Tanaka T. Production of microzonation maps and reports of Anatolian side. Technical report, Istanbul Metropolitan Municipality, department of earthquake risk management and urban development, directorate of earthquake and ground analysis and OYO International Corporation, 2009.

[17] Harmandar E. Spatial Variation of Ground Motion. PhD thesis, Boğaziçi University, 2009.

[18] Kalafat D. Türkiye ve çevresi faylanma - kaynak parametreleri (MT) kataloğu (1938-2008). Boğaziçi Üniversitesi Yayınevi, 2009.

[19] GFZ Potsdam, GEOFON Program Webpage. http://geofon.gfz-potsdam.de/eqinfo/event.php?id=gfz2013xfgj.

Last visited: 19.11.2015.

[20] Harmandar E, Çaktı E, Erdik M. A method for spatial estimation of peak ground acceleration in dense arrays. Geophysical Journal International. 2012; 191(3): 1272-1284.

[21] Boore DM. On pads and filters: processing strong-motion data. Bull Seismol Soc Am. 2005; 95(2): 745–750.

[22] Massa M, Pacor F, Luzi L, Bindi D. The ITalian ACcelerograms Archive (ITACA): processing of strong-motion data. Bull Seismol Soc Am. 2010; 8: 1175–1187.

[23] Kalkan E, Gülkan P. Site-dependent spectra derived from ground motion records in Turkey. Earthquake Spectra. 2004; 20, 1111–1138.

[24] Özbey C, Sari A, Manuel L, Erdik M, Fahjan Y. An empirical attenuation relationship for northwestern Turkey ground motion using a random effects approach. Soil Dyn Earthq Eng. 2004; 24: 115–125.

[25] Kawakami H, Mogi H. Analyzing spatial intraevent variability of peak ground accelerations as a function of separation distance, Bull Seismol Soc Am. 2003; 93: 1079–1090.

[26] Boore DM, Gibbs JF, Joyner WB, Tinsley JC, Ponti DJ. Estimated ground motion from the 1994 Northridge, California, earthquake at the site of the interstate 10 and la cienega boulevard bridge collapse, west Los Angeles, California. Bull Seismol Soc Am. 2003; 93(6): 2737–2751.

[27] Hong HP, Zang Y, Goda K. Effect of spatial correlation on estimated ground-motion prediction equations. Bull Seismol Soc Am. 2009; 99(2A): 928–934.

[28] Esposito S, Iervolino I. Spatial correlation of spectral acceleration in European data. Bull Seismol Soc Am. 2012; 102 (6): 2781–2788.

[29] Daniell JE. Open source procedure for assessment of loss using global earthquake modelling – OPAL-GEM Project. CEDIM Research Report Karlsruhe, Germany. 2009; 09/01.

[30] Daniell JE. open source procedure for assessment of loss using global earthquake modelling software (OPAL). Natural Hazards and Earth System Sciences. 2011; 11: 1885-1900.

[31] Molina S, Lang DH, Lindholm CD. SELENA - An open-source tool for seismic risk and loss assessment using a logic tree computation procedure. Computers & Geosciences. 2010; 36(3): 257-269.

[32] Loth C, Baker JW. A spatial cross-correlation model of spectral accelerations at multiple periods. Earthq Eng Struct Dyn. 2013; 42: 397–417.